High-Pressure Preparation, Crystal Structure, and Properties of α-$(RE)_2B_4O_9$ (RE = Eu, Gd, Tb, Dy): Oxoborates Displaying a New Type of Structure with Edge-Sharing BO_4 Tetrahedra**

Holger Emme and Hubert Huppertz*[a]

Abstract: High-pressure/high-temperature conditions of 10 GPa and 1150 °C were used to synthesize the new rare-earth oxoborates α-$(RE)_2B_4O_9$ (RE = Eu, Gd, Tb, Dy) in a Walker-type multi-anvil apparatus. Single-crystal X-ray structure determination of α-$(RE)_2B_4O_9$ (RE = Eu, Gd, Tb) revealed: *C*2/*c*, $Z = 20$, α-$Eu_2B_4O_9$: $a = 2547.9(5)$, $b = 444.3(1)$, $c = 2493.8(5)$ pm, $\beta = 99.82(3)°$, $R1 = 0.0277$, $wR2 = 0.0693$ (all data); α-$Gd_2B_4O_9$: $a = 2539.0(1)$, $b = 443.3(1)$, $c = 2490.8(1)$ pm, $\beta = 99.88(1)°$, $R1 = 0.0457$, $wR2 = 0.0643$ (all data); α-$Tb_2B_4O_9$: $a = 2529.4(1)$, $b = 441.6(1)$, $c = 2484.3(1)$ pm, $\beta = 99.88(1)°$, $R1 = 0.0474$, $wR2 = 0.0543$ (all data). The isotypic compounds exhibit a new type of structure that is built up of BO_4 tetrahedra to form a network that incorporates the rare-earth cations. The most important feature is the existence of the new structural motif of edge-sharing BO_4 tetrahedra next to the known motif of corner-sharing BO_4 tetrahedra, which is realized in the presented compounds α-$(RE)_2B_4O_9$ (RE = Eu, Gd, Tb, Dy) for the second time. Furthermore, we report the temperature-resolved in-situ powder-diffraction measurements, DTA, IR/Raman spectroscopic investigations, and magnetic properties of the new compounds.

Keywords: borates · fundamental building blocks · high-pressure chemistry · lanthanides · solid-state structures

Introduction

The structural chemistry of oxoborates exhibits a considerable diversity that results from the ability of boron to bind to three or four oxygen atoms to form BO_3 or BO_4 groups. These groups can occur isolated or linked to groups, chains, bands, sheets, or complex networks leading to a great structural diversity.[1, 2] In principle, the structural characteristics are analogous to those of the silicates with the triangular BO_3 group as an additional structural component. In the past seven decades, nearly 500 oxoborates have been structurally characterized. As a common feature of these oxoborates it can be pointed out that the BO_3 triangles and the BO_4 tetrahedra link to each other only through common corners (oxygen atoms) and not through common edges or faces. This characteristic was already postulated in 1967 by Ross and Edwards and was still valid up until a short while ago.[3, 4] The use of high pressures (8 GPa) and high temperatures (1000 °C) during the synthesis enabled us to synthesize the oxoborates $(RE)_4B_6O_{15}$ (RE = Dy, Ho), which are the first examples of borates with edge-sharing BO_4 tetrahedra.[5, 6]

Next to the new structural feature of edge-sharing BO_4 tetrahedra, these compounds also have a new composition with a molar ratio of $(RE)_2O_3$:$B_2O_3 = 2$:3. Known compositions in the system $(RE)_2O_3/B_2O_3$ are $(RE)_3BO_6$ (3:1) (which can be regarded as orthoborates ($[(RE)O]_3BO_3$)), the orthoborates $(RE)BO_3$ (1:1), and the metaborates $(RE)B_3O_6$ (1:3) ($(RE)(BO_2)_3$).[7] While the orthoborates $(RE)BO_3$[8–24] and the metaborates $(RE)B_3O_6$[25–31] have well-defined compositions, several uncertainties concerning the rare earth borates $(RE)_3BO_6$ exist.[7, 32–35] Until now, experiments to synthesize an oxoborate with the composition $(RE)_4B_6O_{15}$ at normal pressures were unsuccessful and led directly to the orthoborates $(RE)BO_3$ and additional B_2O_3.[36] Pressure is evidently a suitable parameter to vary in order to obtain new compositions in oxoborate chemistry. As this substance class exhibits interesting properties, for example, materials for second harmonic generation or host materials for fluorescence, the extension of possible compositions with new structural features provides distinctive opportunities for the discovery and identification of new compounds.[37–39]

[a] Dr. H. Huppertz, Dipl. Chem. H. Emme
Department Chemie
Ludwig-Maximilians-Universität München
Butenandtstraße 5 – 13 (Haus D)
81377 München (Germany)
Fax.: (+49) 89-2180-77440
E-mail: huh@cup.uni-muenchen.de

[**] Throughout this manuscript in the chemical formulae RE stands for rare earth metal.

 DOI: 10.1002/chem.200204696

In this work, we report on the syntheses, crystal structures, and properties of the isotypic rare earth oxoborates α-$(RE)_2B_4O_9$ (RE = Eu, Gd, Tb, Dy), which represent the second example of a new composition ($(RE)_2O_3$:B_2O_3 = 1:2) in the system $(RE)_2O_3/B_2O_3$ that has been synthesized by use of high pressures. In addition to the new composition, these oxoborates exhibit a new structural type in which edge-sharing of BO_4 tetrahedra is observed for the second time in the structural chemistry of oxoborates. We designated these compounds as α-phases, because in the case of RE = Dy we were able to synthesize a second polymorph β-$Dy_2B_4O_9$ in a flux of B_2O_3/Na_2O_2.[40]

Experimental Section

Preparation: The borates were synthesized according to Equation (1). The starting material for the synthesis of α-$(RE)_2B_4O_9$ (RE = Eu, Gd, Dy) in this work was a 1:2 molar mixture of the rare earth oxides $(RE)_2O_3$ (RE = Eu, Gd, Dy) (99.9%, Sigma-Aldrich, Taufkirchen) with B_2O_3 (from H_3BO_3 (99.8%, Merck, Darmstadt) fired at 600 °C). For the synthesis of α-$Tb_2B_4O_9$ we used a mixture of Tb_4O_7 and B_2O_3 according to Equation (2).

$$(RE)_2O_3 + 2\,B_2O_3 \xrightarrow[1150\,^\circ C]{10.0\,GPa} \alpha\text{-}(RE)_2B_4O_9\ (RE = Eu, Gd, Dy) \quad (1)$$

$$Tb_4O_7 + 4\,B_2O_3 \xrightarrow[1150\,^\circ C]{10.0\,GPa} 2\,\alpha\text{-}Tb_2B_4O_9 + \tfrac{1}{2}O_2 \quad (2)$$

The starting materials were compressed in a multianvil assembly (14/8) with a modified Walker module and a 1000-t press. Precast MgO octahedra (Ceramic Substrates & Components, Isle of Wight, UK) with an edge length of 14 mm were used as a pressure medium. Eight tungsten carbide cubes with a truncation of 8 mm, separated by pyrophyllite gaskets, compressed the octahedra (14/8 assembly in conventional terminology). The mixtures (each ≈60 mg) were filled into cylindrical boron nitride crucibles that were sealed by a boron nitride plate. The sample cylinders were placed at the center of cylindrical resistance heaters (graphite) that had a variable (stepped) wall thickness to minimize the thermal gradient along the sample. MgO rods filled the space on the top and bottom of the samples. Thermal insulation was provided by a cylindrical zirconia sleeve that surrounded the furnace. The assemblies were positioned inside the octahedra and were placed in contact with a molybdenum ring at the top and a molybdenum plate at the bottom. The experimental temperature was monitored by means of a $Pt/Pt_{87}Rh_{13}$ thermocouple that was inserted axially into the octahedral assemblies, with the hot junction in contact with the boron nitride cylinder. More details concerning the construction of the assembly can be found in references [21, 41–43]. For the synthesis of α-$(RE)_2B_4O_9$ (RE = Eu, Gd, Tb, Dy), the assemblies were compressed for 3 h to 10 GPa and heated to 1150 °C in the following 10 min. After holding at this temperature for 10 min, the samples were cooled to room temperature over a further period of 10 min. After decompression, the recovered experimental octahedra were broken apart and the samples carefully separated from the surrounding BN. The oxoborates α-$(RE)_2B_4O_9$ (RE = Gd, Tb, Dy) were obtained as colorless, crystalline phases (≈35 mg per run). In contrast to the single-phase products α-$(RE)_2B_4O_9$ (RE = Gd, Tb, Dy), the powder pattern of α-$Eu_2B_4O_9$ exhibited an additional phase that was identified as EuB_4O_7. Quantitative analysis of α-$(RE)_2B_4O_9$ (RE = Gd, Tb) with respect to the rare earth elements gadolinium, terbium, and boron with ICP (Inductively Coupled Plasma) on a VARIAN-VISTA-Spectrometer led to 62.7 wt% Gd (64.2%)/8.7% B (8.6%) in α-$Gd_2B_4O_9$ and 60.5 wt% Tb (62.9%)/8.6% B (8.6%) in α-$Tb_2B_4O_9$ (theoretical values in parentheses).

X-ray diffraction investigations: The powder diffraction data of α-$(RE)_2B_4O_9$ (RE = Eu, Gd, Tb, Dy) were collected on a STOE Stadi P powder diffractometer with monochromatic $Cu_{K\alpha1}$ radiation. The obtained diffraction patterns were indexed with the program ITO on the basis of a monoclinic unit cell.[44] The lattice parameters (α-$Gd_2B_4O_9$: a = 2538.9(3), b = 443.3(1), c = 2490.8(4), β = 99.88(1)°; α-$Tb_2B_4O_9$: a = 2527.9(6), b = 441.2(1), c = 2482.3(7) pm, β = 99.89(2)° (Table 1); α-$Dy_2B_4O_9$: a = 2520.2(4), b = 440.6(1), c = 2478.2(6) pm, β = 99.90(1)°) were obtained from least-square fits of the powder data. The correct indexing of the patterns was ensured by intensity calculations taking the atomic positions from the structure refinements.[45] The lattice parameters, determined from the powders and the single crystals, agreed well (Table 1). For indexing the isotypic europium phase α-$Eu_2B_4O_9$, which exhibited additional reflections of EuB_4O_7 in the powder pattern, only corresponding reflections were used. The lattice parameters (a = 2547.8(3), b = 444.3(1), c = 2493.0(3) pm, β = 99.80(1)° (Table 1)) were obtained from least-square fits of the corresponding reflections.

Small single crystals of α-$(RE)_2B_4O_9$ (RE = Eu, Gd, Tb) were isolated by mechanical fragmentation and examined by Buerger precession photographs. Single-crystal intensity data were collected from regularly shaped colorless crystals (rods) at room temperature by means of an Enraf-Nonius Kappa CCD equipped with a rotating anode ($Mo_{K\alpha}$ radiation (λ = 71.073 pm)). A numerical absorption correction (HABITUS)[46] was applied to the data. All relevant information concerning the data collection are listed in Table 1. According to the systematic extinctions hkl with $h + k \neq 2n$, $h0l$ with $h,l \neq 2n$, and $0kl$ with $k \neq 2n$, the space groups Cc (No. 9) and $C2/c$ (No. 15) were derived. The centrosymmetric group was found to be correct during the structure refinement, while the noncentrosymmetric solution exhibited negative anisotropic displacement parameters and large correlation matrix elements indicating missing symmetry. This was confirmed with the ADDSYM routine of the program PLATON.[47] The starting positional parameters were deduced from an automatic interpretation of direct methods with SHELXS-97[48] and the structures were successfully refined with anisotropic atomic displacement parameters for all atoms with SHELXL-97 (full-matrix least-squares on F^2).[49] Final difference Fourier syntheses revealed no significant residual peaks in all refinements (see Table 1). The parameters for the single-crystal structure measurements of α-$(RE)_2B_4O_9$ (RE = Eu, Gd, Tb) are listed in Table 1. Because the compounds are isotypic, the positional parameters (Table 2), anisotropic displacement parameters (Table 3), interatomic bond lengths (Tables 4 and 5), and angles (Table 6) were only listed for α-$Gd_2B_4O_9$. Further details on the crystal structure investigations may be obtained from the Fachinformationszentrum Karlsruhe, 76344 Eggenstein-Leopoldshafen, Germany (fax: (+49) 7247-808-666; e-mail: crysdata@fiz-karlsruhe.de), on quoting the depository number CSD – 412898 for α-$Eu_2B_4O_9$, CSD-412896 for α-$Gd_2B_4O_9$, and CSD-412897 for α-$Tb_2B_4O_9$.

Abstract in German: *Mit Hilfe einer Multianvil-Apparatur (Walker-Typ) gelang uns unter Hochdruck/Hochtemperatur-Bedingungen von 10 GPa und 1150 °C die Synthese der neuen Selten-Erd Oxoborate α-$(RE)_2B_4O_9$ (RE = Eu, Gd, Tb, Dy). Die Röntgenstrukturanalyse an Einkristallen zeigt, dass die Verbindungen monoklin mit den folgenden Parametern kristallisieren: C2/c, Z = 20, α-$Eu_2B_4O_9$: a = 2547,9(5), b = 444,3(1), c = 2493,8(5) pm, β = 99,82(3)°, R1 = 0,0277, wR2 = 0,0693 (alle Daten); α-$Gd_2B_4O_9$: a = 2539,0(1), b = 443,3(1), c = 2490,8(1) pm, β = 99,88(1)°, R1 = 0,0457, wR2 = 0,0643 (alle Daten); α-$Tb_2B_4O_9$: a = 2529,4(1), b = 441,6(1), c = 2484,3(1) pm, β = 99,88(1)°, R1 = 0,0474, wR2 = 0,0543 (alle Daten). Die isotypen Verbindungen weisen einen neuen Strukturtyp auf, welcher aus einem Netzwerk von BO_4-Tetraedern aufgebaut ist, in dem die Seltenerd-Kationen eingelagert sind. Das herausragendste Merkmal dieser Struktur ist das Strukturmotiv kantenverknüpfter BO_4-Tetraeder, welches in den neuen Verbindungen α-$(RE)_2B_4O_9$ (RE = Eu, Gd, Tb, Dy) erst zum zweiten Mal beobachtet wird. Weiterhin berichten wir über temperaturabhängige in-situ Pulverbeugungsexperimente, DTA, IR/Raman und magnetische Untersuchungen an den neuen Verbindungen.*

Table 1. Powder diffraction, single-crystal data, and structure refinement for α-$(RE)_2B_4O_9$ (RE = Eu, Gd, Tb).

	α-$Eu_2B_4O_9$	α-$Gd_2B_4O_9$	α-$Tb_2B_4O_9$
M_r [g mol^{-1}]	491.16	501.74	505.08
crystal system	monoclinic	monoclinic	monoclinic
space group	*C*2/*c* (No. 15)	*C*2/*c* (No. 15)	*C*2/*c* (No. 15)
powder diffraction data			
a [pm]	2547.8(3)	2538.9(3)	2527.9(6)
b [pm]	444.3(1)	443.3(1)	441.2(1)
c [pm]	2493.0(3)	2490.8(4)	2482.3(7)
β [°]	99.80(1)	99.88(1)	99.89(2)
V [nm^3]	2.781(1)	2.761(1)	2.728(1)
single-crystal data			
a [pm]	2547.9(5)	2539.0(1)	2529.4(1)
b [pm]	444.3(1)	443.3(1)	441.6(1)
c [pm]	2493.8(5)	2490.8(1)	2484.3(1)
β [°]	99.82(3)	99.88(1)	99.88(1)
Z	20	20	20
T [K]	293(2)	293(2)	293(2)
ρ [g cm^{-3}]	5.864	6.034	6.136
crystal size [mm]	0.06 × 0.04 × 0.03	0.04 × 0.02 × 0.01	0.04 × 0.02 × 0.02
detector distance [mm]	35.0	30.0	30.0
exposure time [s °$^{-1}$]	180	60	220
μ [mm^{-1}]	22.37	23.84	25.69
F(000)	4360	4400	4440
θ range [°]	3.3–32.5	3.3–32.5	3.3–37.5
hkl range	−37/+38, ±6, ±37	±38, ±6, ±37	±42, ±7, ±42
scan type	φ/ω	φ/ω	φ/ω
reflections	34418	32091	45034
independent reflections	5038 (R_{int} = 0.0898)	5011 (R_{int} = 0.0642)	7203 (R_{int} = 0.0628)
observed reflections [$I > 2\sigma(I)$]	4710 (R_σ = 0.0432)	4062 (R_σ = 0.0505)	5785 (R_σ = 0.0534)
data/parameters	5038/340	5011/340	7203/340
absorption correction		numerical (HABITUS[46])	
min./max. transmission ratio	0.91/0.99	0.52/0.70	0.50/0.62
GOF on F^2	1.135	1.070	1.029
final *R* indices [$I > 2\sigma(I)$]			
*R*1	0.0250	0.0306	0.0306
*wR*2	0.0657	0.0560	0.0506
*R*1 indices (all data)			
*R*1	0.0277	0.0457	0.0474
*wR*2	0.0693	0.0643	0.0543
extinction coefficient	0.00048(1)	0.00012(1)	0.00013(1)
largest diff. peak/hole [e Å^{-3}]	3.52/−2.09	2.55/−2.63	2.37/−1.98

Results and Discussion

Figure 1 gives a view of the crystal structure of α-$(RE)_2B_4O_9$ (RE = Eu, Gd, Tb, Dy) along [0 1 0]. The structure exhibits a complex network of linked BO_4 tetrahedra. This new structure of α-$(RE)_2B_4O_9$ (RE = Eu, Gd, Tb, Dy) is the second example after $(RE)_4B_6O_{15}$ (RE = Dy, Ho)[5, 6] of an oxoborate in which the BO_4 tetrahedra are linked by common corners as well as by common edges. For a clearer representation, the corner-sharing tetrahedra are drawn as light polyhedra and the edge-sharing tetrahedra as black polyhedra. Figure 2 represents the centrosymmetric fundamental building block consisting of 18 corner-sharing and two edge-sharing BO_4 tetrahedra.

In the last decade, a new fundamental building block (FBB) concept was introduced by Burns, Grice, and Hawthorne that struck a successful balance between the amount of information conveyed and the complexity of the descriptor.[50, 51] Although this method does not always result in a unique descriptor for the fundamental building block, it does provide considerably more information than previous schemes. The

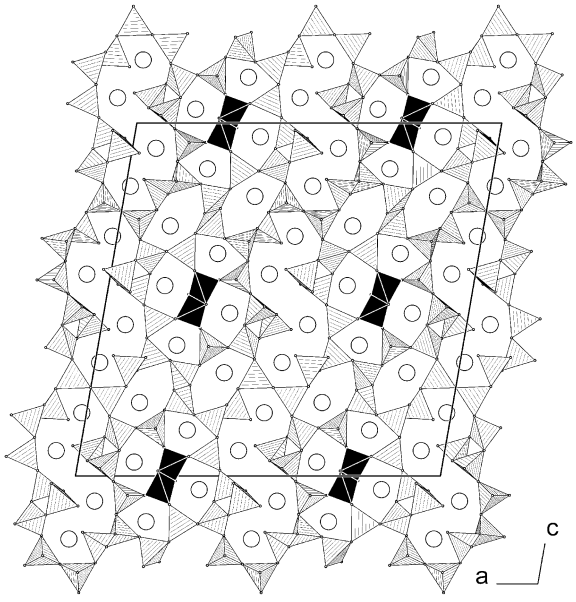

Figure 1. Crystal structure of α-$(RE)_2B_4O_9$ (RE = Eu, Gd, Tb, Dy), view along [0 1 0].

Table 2. Atomic coordinates and isotropic equivalent displacement parameters U_{eq} [Å^2] for α-$Gd_2B_4O_9$ (space group $C2/c$). U_{eq} is defined as one third of the trace of the orthogonalized U_{ij} tensor.

Atom	Wyckoff position	x	y	z	U_{eq}
Gd1	8*f*	0.06461(2)	0.20268(7)	0.07152(2)	0.00615(7)
Gd2	8*f*	0.21555(2)	0.20561(7)	0.12986(2)	0.00685(7)
Gd3	8*f*	0.01244(2)	0.67098(7)	0.17880(2)	0.00597(7)
Gd4	8*f*	0.35900(2)	0.17638(7)	0.20786(2)	0.00749(7)
Gd5	8*f*	0.15455(2)	0.22907(7)	0.96094(2)	0.01070(8)
B1	8*f*	0.2417(3)	0.722(2)	0.0382(3)	0.007(2)
B2	8*f*	0.2511(3)	0.172(2)	0.2815(3)	0.007(2)
B3	8*f*	0.9275(3)	0.300(2)	0.0301(3)	0.006(2)
B4	8*f*	0.1473(3)	0.721(2)	0.0581(3)	0.007(2)
B5	8*f*	0.0991(3)	0.172(2)	0.1927(3)	0.007(2)
B6	8*f*	0.3545(3)	0.193(2)	0.3368(3)	0.007(2)
B7	8*f*	0.9482(3)	0.179(2)	0.2254(3)	0.005(2)
B8	8*f*	0.3046(3)	0.659(2)	0.1330(3)	0.008(2)
B9	8*f*	0.9697(3)	0.815(2)	0.0652(3)	0.008(2)
B10	8*f*	0.9084(3)	0.130(2)	0.1236(3)	0.007(2)
O1	8*f*	0.2712(2)	0.525(1)	0.0813(2)	0.0065(8)
O2	8*f*	0.1988(2)	0.884(1)	0.0551(2)	0.0061(8)
O3	8*f*	0.2235(2)	0.562(1)	0.9861(2)	0.0075(8)
O4	8*f*	0.0626(2)	0.379(1)	0.9787(2)	0.0061(8)
O5	8*f*	0.4040(2)	0.790(1)	0.2534(2)	0.0067(8)
O6	4*e*	0	0.318(2)	$^1/_4$	0.006(2)
O7	8*f*	0.0622(2)	0.144(1)	0.8891(2)	0.0067(8)
O8	8*f*	0.0212(2)	0.690(1)	0.0852(2)	0.0076(8)
O9	8*f*	0.3810(2)	0.354(1)	0.2990(2)	0.0080(8)
O10	8*f*	0.3702(2)	0.327(1)	0.3909(2)	0.0069(8)
O11	8*f*	0.9744(2)	0.120(1)	0.0428(2)	0.0060(8)
O12	8*f*	0.9351(2)	0.3136(9)	0.1689(2)	0.0044(8)
O13	8*f*	0.1065(2)	0.852(1)	0.0157(2)	0.0059(8)
O14	8*f*	0.1527(2)	0.405(1)	0.0556(2)	0.0074(8)
O15	8*f*	0.1080(2)	0.701(1)	0.9274(2)	0.0064(8)
O16	8*f*	0.0466(2)	0.176(1)	0.1596(2)	0.0081(9)
O17	8*f*	0.2956(2)	0.238(1)	0.3270(2)	0.0084(9)
O18	8*f*	0.3028(2)	0.970(1)	0.1336(2)	0.0084(9)
O19	8*f*	0.9483(2)	0.858(1)	0.2263(2)	0.0062(8)
O20	8*f*	0.2126(2)	0.021(1)	0.3131(2)	0.0076(8)
O21	8*f*	0.2295(2)	0.458(2)	0.2569(2)	0.0117(9)
O22	8*f*	0.3638(2)	0.861(1)	0.3354(2)	0.0085(9)
O23	8*f*	0.3574(2)	0.506(1)	0.1361(2)	0.0065(8)

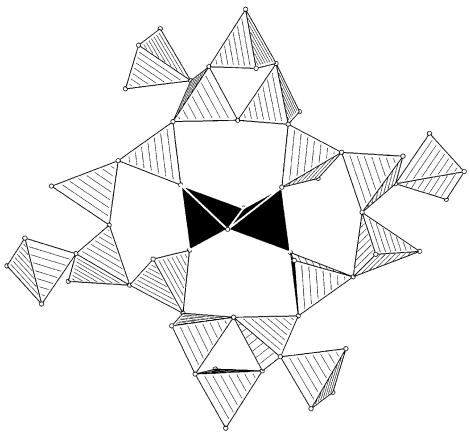

20□:[◪]=<4□◪>=<3□>□|-<5□>□|=<4□◪>=<3□>□|-<5□>□|

Figure 2. Fundamental building block of α-$(RE)_2B_4O_9$ (RE = Eu, Gd, Tb, Dy).

concept of Burns et al. is based on the assumption that the polymerization of adjacent polyhedra involves corner-sharing only. As we were able to synthesize oxoborates exhibiting edge-sharing BO_4 tetrahedra,[5, 6] the known descriptors used by Burns et al. had to be extended with a symbol for this new structural motif. For geometrical and graphical reasons, we introduced the new descriptor ◪ for two edge-sharing BO_4 tetrahedra.[6] This symbol can be used to describe the fundamental building block of α-$(RE)_2B_4O_9$ (RE = Eu, Gd, Tb, Dy) with the descriptor 20□:[◪] = ⟨4□ ◪⟩ = ⟨3□⟩□| − ⟨5□⟩□| = ⟨4□◪⟩ = ⟨3□⟩□| − ⟨5□⟩□| . In detail, the edge-sharing tetrahedra represent the centre of the FBB "[◪]". On each of the two longer sides of this center, a six-membered ring ⟨4□ ◪⟩ is built by four additional corner-sharing tetrahedra. On each of the shorter sides, one of the edge-sharing tetrahedra builds a five-membered ring with four additional corner-sharing tetrahedra ⟨5□⟩, from which two tetrahedra already belong to the six-membered rings on the longer sides. On the outer side of the six-membered rings, an additional three-membered ring ⟨3□⟩ is built by means of two common corner-sharing tetrahedra. Both, the six- and five-membered rings are additionally connected to a single outer tetrahedron □ in such a way that the centrosymmetry of the fundamental building block is fulfilled.

The fundamental building blocks are linked together by the single outer tetrahedron and the one tetrahedron of the five-membered rings, which is neither linked to the single outer tetrahedron nor is part of one of the six-membered rings. The linkage of the fundamental building blocks gives rise to further rings. Additional seven-membered rings on the sides of the five-membered rings and additional fourteen-membered rings on the sides of the six-membered rings form a stretched "S" (Figure 1). These rings form planes that are linked to the corresponding planes above and below. The complex connection of these planes forms even more rings.

To examine the ring sizes topologically, we calculated the cycle class sequence for α-$(RE)_2B_4O_9$ (RE = Eu, Gd, Tb) specifying the relative abundance of B_nO_n ring sizes (for n = 2 – 19) per unit cell.[52–55] The results are given in Table 7.

The rare earth ions (Eu^{3+}, Gd^{3+}, Tb^{3+}, Dy^{3+}) are positioned in the channels formed by the ring system. The five crystallographically different RE^{3+} ions are surrounded by 8, 9, 10, or 11 oxygen atoms (Figure 3). In the case of $RE^{3+} = Gd^{3+}$, the bond lengths in the coordination polyhedra vary between 225 and 306 pm (Table 5). For α-$Eu_2B_4O_9$ and α-$Tb_2B_4O_9$ the bond lengths lie in the range 226 – 304 pm and 223 – 307 pm, respectively.

The B – O bond lengths in α-$(RE)_2B_4O_9$ (RE = Eu, Gd, Tb) vary between 139 – 159 pm (α-$Eu_2B_4O_9$), 138 – 160 pm (α-$Gd_2B_4O_9$), and 139 – 158 pm (α-$Tb_2B_4O_9$). The highest and the lowest bond lengths slightly exceed the typical B – O bond lengths in BO_4 tetrahedra.[56] Both bond lengths appear in the tetrahedron B8, which is directly linked to the edge-sharing tetrahedra. A view of the thermal ellipsoids around B8 in α-$Gd_2B_4O_9$ shows no discrepancies in their dimensions (Figure 4). Despite of the large ranges, the average B – O bond lengths with the values 148.0 pm (RE = Eu), 147.9 pm (RE = Gd) (Table 4), and 147.8 pm (RE = Tb) correspond to the known average value of 147.6 pm for oxoborates.[56] The O-B-O

Table 3. Anisotropic displacement parameters [Å^2] for α-$Gd_2B_4O_9$ (space group $C2/c$).

Atom	U_{11}	U_{22}	U_{33}	U_{12}	U_{13}	U_{23}
Gd1	0.0058(2)	0.0072(2)	0.0056(2)	0.0008(1)	0.0014(1)	0.0007(1)
Gd2	0.0066(2)	0.0061(2)	0.0081(2)	0.0000(1)	0.0018(2)	−0.0002(1)
Gd3	0.0070(2)	0.0058(2)	0.0055(2)	0.0001(1)	0.0021(1)	−0.0001(1)
Gd4	0.0078(2)	0.0075(2)	0.0069(2)	0.0006(2)	0.0004(2)	0.0008(2)
Gd5	0.0081(2)	0.0097(2)	0.0144(2)	−0.0010(2)	0.0022(2)	−0.0043(2)
B1	0.005(3)	0.008(3)	0.007(3)	0.002(2)	0.001(2)	−0.003(2)
B2	0.004(3)	0.008(3)	0.008(3)	0.000(2)	0.001(2)	−0.002(2)
B3	0.008(3)	0.005(3)	0.004(3)	0.001(2)	0.002(2)	0.001(2)
B4	0.008(3)	0.005(3)	0.009(3)	0.002(2)	0.000(2)	−0.001(2)
B5	0.008(3)	0.007(3)	0.008(3)	0.000(2)	0.006(2)	0.001(2)
B6	0.009(3)	0.007(3)	0.005(3)	0.000(2)	0.000(2)	0.000(2)
B7	0.005(3)	0.004(3)	0.005(3)	0.002(2)	0.001(2)	0.002(2)
B8	0.006(3)	0.008(3)	0.011(3)	0.002(2)	0.002(3)	0.000(3)
B9	0.005(3)	0.008(3)	0.012(3)	−0.001(2)	−0.001(2)	−0.001(3)
B10	0.005(3)	0.005(3)	0.011(3)	0.000(2)	0.004(2)	−0.003(2)
O1	0.006(2)	0.007(2)	0.005(2)	−0.001(2)	−0.001(2)	0.001(2)
O2	0.005(2)	0.006(2)	0.007(2)	0.001(2)	0.000(2)	−0.002(2)
O3	0.008(2)	0.008(2)	0.007(2)	−0.002(2)	0.002(2)	−0.003(2)
O4	0.008(2)	0.006(2)	0.004(2)	0.000(2)	−0.003(2)	0.002(2)
O5	0.007(2)	0.008(2)	0.006(2)	0.006(2)	0.003(2)	0.002(2)
O6	0.008(3)	0.005(3)	0.005(3)	0	0.000(2)	0
O7	0.007(2)	0.006(2)	0.006(2)	0.003(2)	0.001(2)	0.002(2)
O8	0.008(2)	0.007(2)	0.010(2)	0.002(2)	0.006(2)	0.001(2)
O9	0.013(2)	0.006(2)	0.005(2)	0.000(2)	0.001(2)	−0.002(2)
O10	0.007(2)	0.007(2)	0.006(2)	−0.003(2)	−0.001(2)	−0.001(2)
O11	0.008(2)	0.006(2)	0.005(2)	−0.001(2)	0.002(2)	−0.000(2)
O12	0.005(2)	0.003(2)	0.004(2)	−0.002(2)	−0.001(2)	0.001(2)
O13	0.007(2)	0.006(2)	0.005(2)	0.000(2)	0.000(2)	0.000(2)
O14	0.007(2)	0.008(2)	0.007(2)	−0.001(2)	0.000(2)	−0.002(2)
O15	0.004(2)	0.009(2)	0.006(2)	0.004(2)	0.000(2)	0.004(2)
O16	0.010(2)	0.009(2)	0.004(2)	−0.002(2)	−0.001(2)	0.000(2)
O17	0.002(2)	0.010(2)	0.013(2)	−0.001(2)	0.000(2)	−0.004(2)
O18	0.010(2)	0.006(2)	0.010(2)	0.001(2)	0.001(2)	0.000(2)
O19	0.004(2)	0.007(2)	0.008(2)	−0.002(2)	0.001(2)	0.002(2)
O20	0.008(2)	0.008(2)	0.007(2)	−0.002(2)	0.001(2)	−0.002(2)
O21	0.014(2)	0.012(2)	0.011(2)	0.003(2)	0.007(2)	0.004(2)
O22	0.010(2)	0.006(2)	0.011(2)	0.001(2)	0.008(2)	0.000(2)
O23	0.004(2)	0.010(2)	0.006(2)	0.003(2)	0.001(2)	0.001(2)

Table 4. Interatomic bond lengths [pm] calculated with the single-crystal lattice parameters in α-$Gd_2B_4O_9$ (standard deviations in parentheses).[a]

B1–B1	204(2)						
B1–O2	142.6(8)	B2–O21	148.8(8)	B3–O11	142.4(8)	B4–O14	140.7(8)
B1–O1	148.4(8)	B2–O17	148.5(8)	B3–O4	146.8(8)	B4–O13	146.7(8)
B1–O3a	150.1(8)	B2–O21	147.3(8)	B3–O13	147.1(8)	B4–O10	149.2(8)
B1–O3b	148.1(8)	B2–O20	151.5(8)	B3–O15	150.4(8)	B4–O2	150.7(8)
	∅147.3		∅149.0		∅146.7		∅146.8
B5–O16	144.4(8)	B6–O9	143.8(8)	B7–O19	142.1(8)	B8–O18	137.8(8)
B5–O5	145.6(8)	B6–O10	146.4(8)	B7–O12	151.4(8)	B8–O23	149.5(8)
B5–O9	149.8(8)	B6–O17	148.7(8)	B7–O6	148.6(7)	B8–O1	153.6(8)
B5–O22	151.8(8)	B6–O22	149.2(8)	B7–O5	150.3(8)	B8–O20	160.2(9)
	∅147.9		∅147.0		∅148.1		∅150.3
B9–O8	142.8(8)	B10–O15	147.2(8)				
B9–O11	147.7(8)	B10–O12	145.8(8)				
B9–O7	151.6(9)	B10–O7	149.1(8)				
B9–O4	151.5(8)	B10–O23	148.9(8)				
	∅148.4		∅147.8				

[a] Average of all B–O bond lengths: 147.9 pm.

angles in the corner-sharing BO_4 tetrahedra vary between 99.5–118.9° for α-$Eu_2B_4O_9$, 99.4–119.0° for α-$Gd_2B_4O_9$ (Table 6), and 99.4–119.4° for α-$Tb_2B_4O_9$. The B–O bond lengths and angles in the edge-sharing BO_4 tetrahedra (Figure 5) are of special interest. Table 8 gives a comparison between the data of α-$(RE)_2B_4O_9$ (RE = Eu, Gd, Tb) and that of $(RE)_4B_6O_{15}$ (RE = Dy, Ho). The B···B distances in the edge-sharing tetrahedra are 204(2) pm in α-$Gd_2B_4O_9$, 205.3(9) pm in α-$Eu_2B_4O_9$, and 205.9(9) pm in α-$Tb_2B_4O_9$. These are even shorter than in $(RE)_4B_6O_{15}$ (RE = Dy, Ho)

Table 5. Interatomic Gd–O bond lengths [pm] calculated with the single-crystal lattice parameters in α-$Gd_2B_4O_9$ (standard deviations in parentheses).[a]

Gd1–O11	230.7(4)	Gd2–O2	232.6(4)	Gd3–O19	232.4(4)	Gd4–O5	225.2(4)	Gd5–O3	229.3(4)
Gd1–O16	232.0(4)	Gd2–O17a	237.4(4)	Gd3–O8	238.1(4)	Gd4–O23	230.3(4)	Gd5–O15a	247.6(4)
Gd1–O10	242.1(4)	Gd2–O14	239.5(4)	Gd3–O6	242.6(4)	Gd4–O18	232.1(4)	Gd5–O14	249.2(4)
Gd1–O4	243.2(4)	Gd2–O22	242.5(4)	Gd3–O16a	243.7(5)	Gd4–O20	236.3(4)	Gd5–O4	253.8(4)
Gd1–O13	244.9(4)	Gd2–O18	243.7(4)	Gd3–O7	245.4(4)	Gd4–O19	237.5(4)	Gd5–O1	257.0(4)
Gd1–O8a	247.6(4)	Gd2–O1	245.9(4)	Gd3–O16b	247.6(4)	Gd4–O9	237.7(4)	Gd5–O13	259.1(4)
Gd1–O14	250.4(4)	Gd2–O20	253.2(4)	Gd3–O12	250.1(4)	Gd4–O21	272.6(5)	Gd5–O23	260.1(4)
Gd1–O8b	257.3(4)	Gd2–O17b	262.8(5)	Gd3–O19	254.2(4)	Gd4–O12	281.3(4)	Gd5–O15b	269.0(4)
Gd1–O22	278.0(5)	Gd2–O10	272.7(4)	Gd3–O9	278.9(5)			Gd5–O7	272.1(4)
				Gd3–O5	299.5(4)			Gd5–O2	286.2(4)
								Gd5–O18	306.0(4)
	∅247.4		∅247.8		∅253.3		∅244.1		∅262.7

[a] Average of all bond lengths: 251.7 pm.

Table 6. Interatomic angles [°] calculated with the single-crystal lattice parameters in α-$Gd_2B_4O_9$ (standard deviations in parentheses).

B1-O3-B1	86.1(5)				
O2-B1-O3b	111.1(5)	O21-B2-O17	109.2(5)	O11-B3-O4	114.7(5)
O2-B1-O1	113.6(5)	O21a-B2-O21b	115.0(5)	O11-B3-O13	105.9(5)
O3b-B1-O1	113.2(5)	O17-B2-O21b	108.9(5)	O4-B3-O13	115.0(5)
O2-B1-O3a	109.3(5)	O21a-B2-O20	111.7(5)	O11-B3-O15	114.9(5)
O3b-B1-O3a	93.9(5)	O17-B2-O20	99.4(5)	O4-B3-O15	104.3(5)
O1-B1-O3a	114.1(5)	O21b-B2-O20	111.4(5)	O13-B3-O15	101.5(5)
	∅109.2		∅109.3		∅109.4
O14-B4-O13	115.0(5)	O16-B5-O5	109.4(5)	O9-B6-O10	108.5(5)
O14-B4-O10	113.4(5)	O16-B5-O9	110.4(5)	O9-B6-O17	113.3(5)
O13-B4-O10	102.2(5)	O5-B5-O9	106.4(5)	O10-B6-O17	101.7(5)
O14-B4-O2	112.6(5)	O16-B5-O22	108.4(5)	O9-B6-O22	112.4(5)
O13-B4-O2	106.5(5)	O5-B5-O22	111.2(5)	O10-B6-O22	113.8(5)
O10-B4-O2	106.2(5)	O9-B5-O22	111.2(5)	O17-B6-O22	106.7(5)
	∅109.3		∅109.5		∅109.4
O19-B7-O6	114.2(5)	O18-B8-O23	119.0(6)	O8-B9-O11	111.0(5)
O19-B7-O5	108.7(5)	O18-B8-O1	112.5(5)	O8-B9-O4	112.4(5)
O6-B7-O5	110.6(5)	O23-B8-O1	103.1(5)	O11-B9-O4	108.3(5)
O19-B7-O12	114.1(5)	O18-B8-O20	111.1(5)	O8-B9-O7	111.0(5)
O6-B7-O12	104.8(5)	O23-B8-O20	98.8(5)	O11-B9-O7	105.3(5)
O5-B7-O12	103.9(5)	O1-B8-O20	111.3(5)	O4-B9-O7	108.5(5)
	∅109.4		∅109.3		∅109.4
O12-B10-O15	114.2(5)				
O12-B10-O23	110.6(5)				
O15-B10-O23	104.0(5)				
O12-B10-O7	115.8(5)				
O15-B10-O7	108.0(5)				
O23-B10-O7	103.1(5)				
	∅109.3				

[a] Average of all O–B–O angles: 109.4°.

Table 7. Cycle-class sequences of α-$(RE)_2B_4O_9$ (RE = Eu, Gd, Tb).[52–55]

n[a]	2	3	4	5	6	7	8	9	10
α-$(RE)_2B_4O_9$	2	4	–	4	12	16	4	36	71
n[a]	11	12	13	14	15	16	17	18	19
α-$(RE)_2B_4O_9$	106	227	434	905	1860	3502	6466	12382	25202

[a] n = ring size.

(207.2(8) and 207(1) pm). The angles in the planar B_2O_2 ring exhibit average values of 86.5° and 93.5° (Table 8). Thus the bond lengths and angles inside the edge-sharing BO_4 tetrahedra of α-$(RE)_2B_4O_9$ (RE = Eu, Gd, Tb) and $(RE)_4B_6O_{15}$ (RE = Dy, Ho) are similar.

For further insight, we calculated bond-valence sums for α-$(RE)_2B_4O_9$ (RE = Eu, Gd, Tb) with the bond-length/bond-strength concept (Table 9).[57, 58] The formal ionic charge of the atoms, acquired by the X-ray structure analysis, are in agreement within the limits of the concept. Additionally, we calculated MAPLE values (Madelung part of lattice energy)[59–61] for α-$(RE)_2B_4O_9$ (RE = Eu, Gd, Tb) to compare them with the MAPLE values from the binary components $(RE)_2O_3$ (RE = Eu, Gd, Tb) and the high-pressure modification B_2O_3-II.[62] We calculated a value of 58715 kJ mol^{-1} for α-$Eu_2B_4O_9$, 58810 kJ mol^{-1} for α-$Gd_2B_4O_9$, and 58909 kJ mol^{-1} for α-$Tb_2B_4O_9$ compared with 58788 kJ mol^{-1} for α-$Eu_2B_4O_9$, 58860 kJ mol^{-1} for α-$Gd_2B_4O_9$, and 58969 kJ mol^{-1} for α-$Tb_2B_4O_9$ starting from the binary oxides ($1 \times (RE)_2O_3$ (RE = Eu (14912 kJ mol^{-1}), Gd (14984 kJ mol^{-1}), Tb (15093 kJ mol^{-1}) + $2 \times B_2O_3$-II (21938 kJ mol^{-1})) resulting in a deviation of 0.12% for α-$Eu_2B_4O_9$, 0.08% for α-$Gd_2B_4O_9$, and 0.10% for α-$Tb_2B_4O_9$.

Table 8. Comparison of the interatomic distances and bond lengths [pm] as well as angles [°] inside the edge-sharing tetrahedra of α-$(RE)_2B_4O_9$ (RE = Eu, Gd, Tb) and $(RE)_4B_6O_{15}$ (RE = Dy, Ho).

	B1 ··· B1	B1 – O3a	B1 – O3b	B1 – O2	B1 – O1	∢B1-O3a-B1	∢O3a-B1-O3b
α-$Eu_2B_4O_9$	205.3(9)	150.5(5)	149.5(5)	142.6(6)	148.4(6)	86.4(3)	93.6(3)
α-$Gd_2B_4O_9$	204(2)	150.1(8)	148.1(8)	142.6(8)	148.4(8)	86.1(5)	93.9(5)
α-$Tb_2B_4O_9$	205.9(9)	150.0(5)	149.5(6)	142.6(6)	147.6(6)	86.9(3)	93.1(3)
$Dy_4B_6O_{15}$[5, 6]	207.2(8)	150.7(5)	153.3(5)	145.4(4)	146.1(5)	85.9(3)	94.1(3)
$Ho_4B_6O_{15}$[6]	207(1)	151.0(8)	153.7(7)	144.3(7)	145.6(7)	85.6(4)	94.4(4)

Table 9. Bond-valence sums in α-$(RE)_2B_4O_9$ (RE = Eu, Gd, Tb) calculated with the bond-length/bond-strength concept (ΣV).[57, 58]

	ΣV		ΣV		ΣV
Eu1	+3.18	Gd1	+3.16	Tb1	+3.18
Eu2	+3.15	Gd2	+3.09	Tb2	+3.12
Eu3	+3.19	Gd3	+3.15	Tb3	+3.12
Eu4	+3.19	Gd4	+3.24	Tb4	+3.22
Eu5	+2.76	Gd5	+2.73	Tb5	+2.68
B1	+3.01		+3.04		+3.04
B2	+2.88		+2.90		+2.88
B3	+3.08		+3.10		+3.10
B4	+3.06		+3.09		+3.09
B5	+3.00		+3.00		+3.00
B6	+3.06		+3.07		+3.08
B7	+2.98		+2.99		+2.99
B8	+2.86		+2.87		+2.90
B9	+2.96		+2.96		+2.97
B10	+3.01		+3.00		+3.04
O1	−1.99		−1.98		−1.98
O2	−2.18		−2.16		−2.17
O3	−1.95		−1.99		−1.95
O4	−2.11		−2.10		−2.09
O5	−2.16		−2.18		−2.16
O6	−2.16		−2.22		−2.16
O7	−1.93		−1.92		−1.94
O8	−1.89		−1.87		−1.89
O9	−2.07		−1.98		−1.93
O10	−2.06		−2.05		−2.10
O11	−2.12		−2.14		−2.16
O12	−1.92		−1.91		−1.94
O13	−2.09		−2.13		−2.09
O14	−1.92		−1.94		−1.93
O15	−2.02		−1.98		−2.00
O16	−2.05		−2.02		−2.03
O17	−2.13		−2.12		−2.11
O18	−1.89		−1.91		−1.88
O19	−2.11		−2.08		−2.03
O20	−1.96		−1.94		−1.99
O21	−1.72		−1.71		−1.69
O22	−1.94		−1.92		−1.94
O23	−2.20		−2.20		−2.22

In-situ powder diffraction and thermoanalytical measurements: To investigate the metastable character of the high-pressure phases α-$(RE)_2B_4O_9$ (RE = Eu, Gd, Tb, Dy), temperature-dependent in-situ X-ray diffractometry was performed on a STOE powder diffractometer Stadi P ($Mo_{K\alpha}$; λ = 71.073 pm) with a computer-controlled STOE furnace. The heating element consisted of an electrically heated graphite tube holding the sample capillary vertically with respect to the scattering plane. Bores in the graphite tube permitted unobstructed pathways for the primary beam and the scattered radiation. The temperature, measured by a thermocouple in the graphite tube, was kept constant to within 0.2 °C.

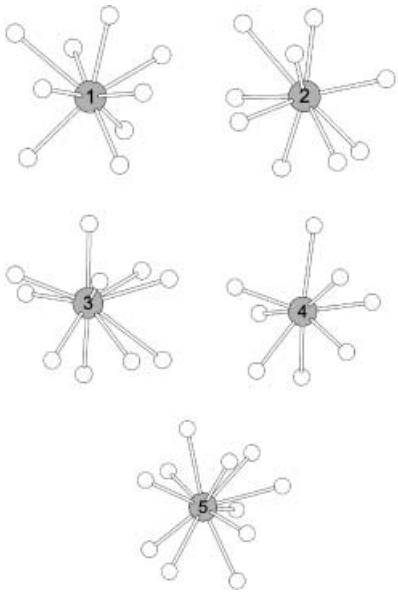

Figure 3. Coordination spheres of RE^{3+} (gray spheres) in the crystal structure of α-$(RE)_2B_4O_9$ (RE = Eu, Gd, Tb, Dy).

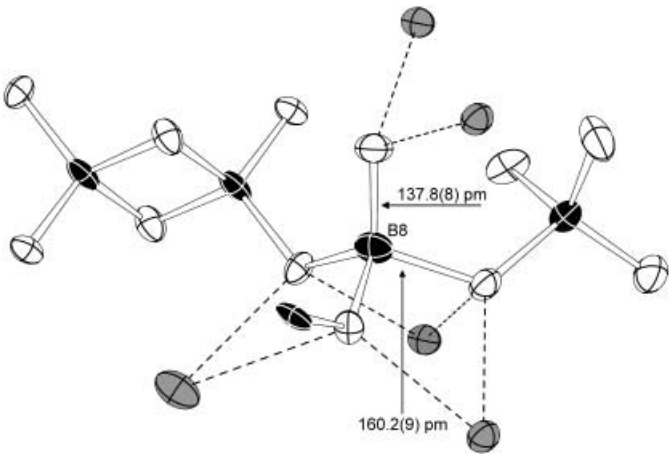

Figure 4. Distortion of the $B(8)O_4$ tetrahedron in α-$Gd_2B_4O_9$ next to the two edge-sharing tetrahedra with thermal ellipsoids given at 70% probability.

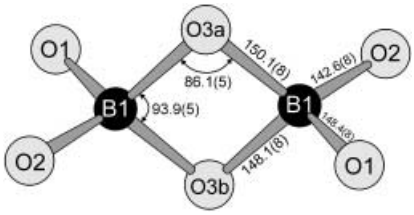

Figure 5. Interatomic bond lengths [pm] and angles [°] inside the edge-sharing BO_4 tetrahedra of α-$Gd_2B_4O_9$.

The heating rate between different temperatures was set to 22 °C min^{-1}. For temperature stabilization, a time of three minutes was given before the start of each data acquisition. Successive heating of the metastable high-pressure phases α-$(RE)_2B_4O_9$ (RE = Eu, Gd, Tb, Dy) in the range of 800 – 900 °C leads to a decomposition into the high-temperature modifications μ-$(RE)BO_3$ (RE = Eu, Gd, Tb, Dy)[8] and molten B_2O_3. Figure 6 shows the results for α-$Gd_2B_4O_9$. Subsequent cooling leads to the complete transformation into the room-temperature modifications π-$(RE)BO_3$ (RE = Eu, Gd, Tb, Dy) between 500 – 600 °C. These results are in agreement with the thermoanalytical measurements performed with a combined DTA-TG thermobalance (TGA 92-2400, Setaram, heating rate: 10 °C min^{-1}) between room temperature and 1000 °C for α-$(RE)_2B_4O_9$ (RE = Eu, Gd, Tb). During heating, broad endothermic effects occur in the DTA between 845 – 886 °C for α-$Eu_2B_4O_9$, 817 – 900 °C for α-$Gd_2B_4O_9$, and 810 – 883 °C for α-$Tb_2B_4O_9$ (Figure 7), owing to decomposition of the compounds.

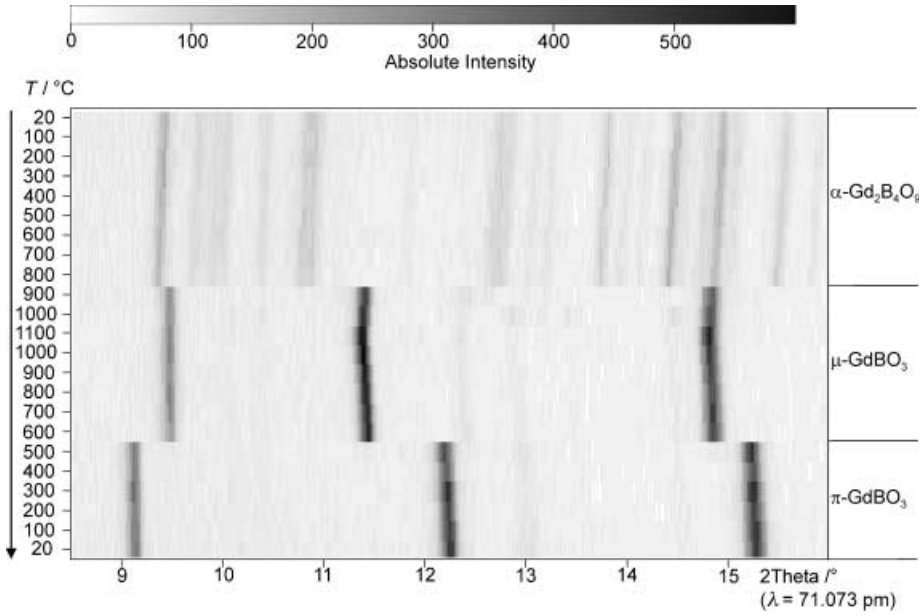

Figure 6. Temperature-dependent X-ray thermodiffractometric powder patterns of the decomposition of α-$Gd_2B_4O_9$.

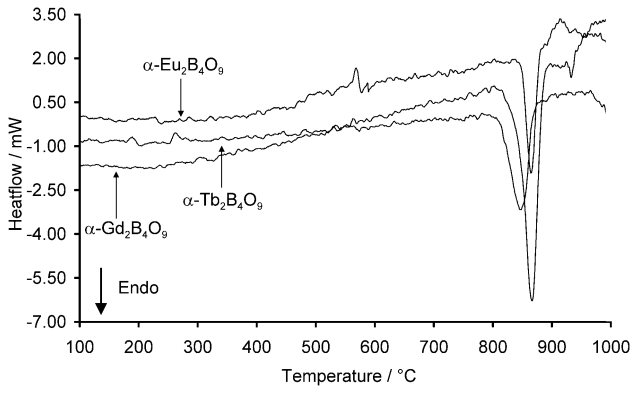

Figure 7. Differential thermal analysis curves of α-$(RE)_2B_4O_9$ (RE = Eu, Gd, Tb) on heating.

Infrared and Raman spectroscopy: The IR spectrum of α-$Gd_2B_4O_9$ was recorded on a Bruker IFS 66v/S spectrometer scanning a range from 400 to 4000 cm^{-1}. The sample was thoroughly mixed with dried KBr (5 mg sample, 500 mg KBr) in a glove box under dried argon atmosphere. The Raman spectrum was measured on a Dilor XY spectrometer with the help of a Raman microscope (Olympus) with an excitation wavelength of 454.5 nm on an aluminum carrier at room temperature (scanning range: 170 – 8000 cm^{-1}). In the upper range of both spectra (4000 – 2000 cm^{-1}), no vibrational bands caused by hydrogen (OH) or water were detectable.

Because the IR spectra of α-$(RE)_2B_4O_9$ (RE = Eu, Tb) show nearly identical absorptions as α-$Gd_2B_4O_9$, only the latter is discussed in the following section. Figures 8 and 9 show the 400 – 2000 cm^{-1} region of the IR and Raman spectrum of α-$Gd_2B_4O_9$. The observed spectral data of α-$Gd_2B_4O_9$ are given in Table 10. Additional data of $Dy_4B_6O_{15}$,[5, 6] including edge-sharing BO_4 tetrahedra, and π-$GdBO_3$,[18, 63] exhibiting exclusively BO_4 tetrahedra in the form of a cyclic B_3O_9 ring, are also given for comparison. In accordance with the crystallographic data, the IR spectrum (Figure 8) only exhibits absorptions typical for BO_4 tetrahedra. Boron, tetrahedrally coordinated to oxygen, displays stretching modes in the region $\nu = 1100$ to 800 cm^{-1} as in π-YBO_3, π-$GdBO_3$, or $TaBO_4$.[13, 64, 65] The most probable assignment is that the bands belonging to the antisymmetric stretching mode are centered at $\tilde{\nu} \approx 1050$ cm^{-1}, while the symmetric stretching frequency is located in the region 900 – 850 cm^{-1}.[66] These stretching modes are split because of the ten crystallographically independent BO_4 tetrahedra in α-$Gd_2B_4O_9$, which are linked through the corners and edges inside the network. Therefore, we observe several broad absorptions that complicate a detailed assignment of the vibrations. We assume that the absorptions at $\nu = 1102$ and 1052 cm^{-1} correspond to antisymmetric stretching modes (1085 and 1010 cm^{-1} in $Dy_4B_6O_{15}$,[6] 1030 and 992 cm^{-1} in π-$GdBO_3$[63]). The Raman spectrum (Figure 9) shows the corresponding total symmetrical stretching modes of the BO_4 tetrahedra at 1084 and 1031 cm^{-1} (1099 and 1008 cm^{-1} in $Dy_4B_6O_{15}$, 1014 and 996 cm^{-1} in π-$GdBO_3$). The symmetric stretching frequencies (ν_s) in the IR spectrum of α-$Gd_2B_4O_9$ presumably lie between 990 and 860 cm^{-1} (between 950 and 790 cm^{-1} in $Dy_4B_6O_{15}$). Furthermore, we observe no significant absorption bands in the range 1450 – 1200 cm^{-1} in the IR spectrum of α-$Gd_2B_4O_9$, which is as expected for oxoborates that do not contain boron in threefold coordination with oxygen atoms. On the other hand, the Raman spectrum

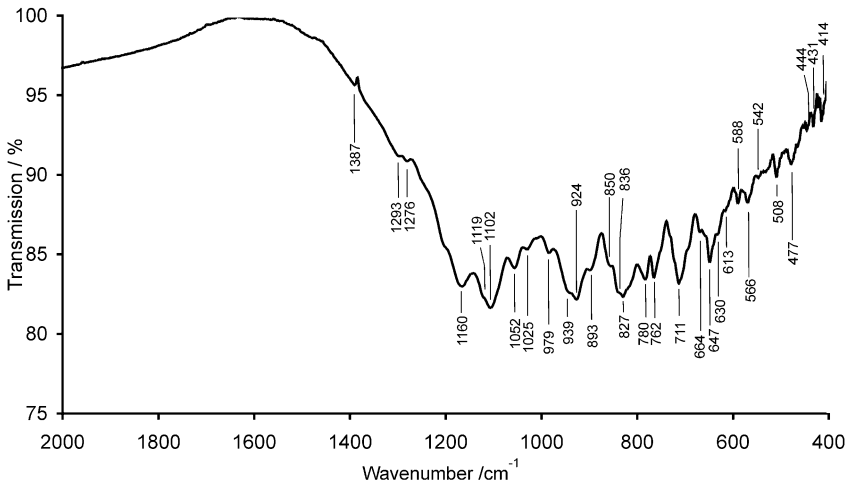

Figure 8. IR spectrum of α-$Gd_2B_4O_9$.

Table 10. Observed vibrational spectral data [cm^{-1}][a] in α-$Gd_2B_4O_9$ in comparison to $Dy_4B_6O_{15}$ and π-$GdBO_3$.[18, 63]

α-$Gd_2B_4O_9$		$Dy_4B_6O_{15}$		π-$GdBO_3$	
IR	Raman	IR	Raman	IR	Raman
	1792 (w, br)				
	1685 (vs)	1634 (vw, br)	1699 (w, br)		
			1519 (w)		
	1431 (vs, br)		1435 (s)		
1387 (vw)		1355 (vw, br)	1384 (s)		
	1340 (m)		1334 (s)		
1293 (vw)			1271 (w)		
1276 (vw)	1253 (m)		1218 (m)		
1160 (s)	1199 (s)		1160 (vs)		
	1147 (s)		1144 (m)		
1119 (sh)	1123 (sh)				
1102 (vs) (ν_{as})	1084 (vs)	1085 (vs, br) (ν_{as})	1099 (m)		
1052 (s) (ν_{as})					
1025 (m, br)	1031 (vs)		1033 (vw)	1030 (ν_{as})	1014
	993 (w)	1010 (s) (ν_{as})	1008 (m)	992 (ν_{as})	996
979 (m, br)	974 (sh)		972 (vw)		
939 (sh)	923 (w)	942 (s, br)	955 (vw)		
924 (vs)	911 (sh)	903 (s, br)		916	
893 (sh)		896 (br)			
850 (m)	869 (vw)				
836 (sh)	830 (vw)	840 (br)		842	
827 (vs)		816 (br)			824
780 (s)		796 (w)			
762 (s)		768 (m)			
		744 (m)		740	
711 (s)		728 (m)			714
		691 (m)		698	
664 (sh)		667 (m)			
647 (s)		646 (sh)			
630 (sh)					
613 (sh)		623 (w)			616
588 (m)		599 (m)			
566 (m)		550 (m)			
542 (sh)		524 (sh)			504
508 (m)		488 (w)			
477 (w)		478 (sh)			
444 (vw)		443 (vw)			
431 (w)		430 (m)		422	432
414 (w)		417 (w)			
		400 (w)		398	410

[a] Abbreviations: s strong; vs very strong; m medium; w weak; vw very weak; br broad; sh shoulder.

exhibits several peaks in this range that are normally correlated to BO_3 groups. As we observe similar new absorption bands in the Raman spectrum of $Dy_4B_6O_{15}$, these bands are probably Raman-active modes of the new B_2O_6 unit of edge-sharing BO_4 tetrahedra inside the BO_4 network.

Magnetic measurements: Magnetic susceptibility measurements were performed on polycrystalline and single-phase samples of α-$(RE)_2B_4O_9$ (RE = Gd, Tb) in a MPMS *XL* SQUID magnetometer (Quantum Design) at temperatures between 2 and 300 K with magnetic flux densities up to 1 T. The measurements were carried out in thin-walled silica tubes.

The temperature-dependence of the inverse magnetic susceptibilities of α-$Gd_2B_4O_9$ and α-$Tb_2B_4O_9$ are presented in Figures 10 and 11. Above 23 K (α-$Gd_2B_4O_9$) and 80 K (α-$Tb_2B_4O_9$), the investigated rare earth oxoborates show Curie–Weiss behavior with experimental magnetic moments of 7.83(1) μ_B per Gd atom and 10.22(1) μ_B per Tb atom. These experimentally determined values are close to the values of 7.94 μ_B and 9.72 μ_B for the free Gd^{3+} and Tb^{3+} ions.[67] The paramagnetic Curie temperatures (Weiss constants) of 15(1) K and 26(1) K were determined by linear extrapolation of the high-temperature parts of the $1/\chi$ versus T plots to $1/\chi = 0$. The positive values indicate predominant paramagnetic interactions (Table 11).

Conclusion

In this paper, we have described the structure and properties of the new rare earth oxoborates α-$(RE)_2B_4O_9$ (RE = Eu, Gd, Tb, Dy) synthesized under high-pressure in a multianvil from the corresponding rare earth oxides (Eu_2O_3, Gd_2O_3, Tb_4O_7, Dy_2O_3) and boron oxide B_2O_3. In addition to the new composition, these isotypic compounds are the second example of an oxoborate structure exhibiting edge-sharing BO_4 tetrahedra. The new structure is built up of a network of corner- and edge-sharing BO_4 tetrahedra. The RE^{3+} (RE = Eu, Gd, Tb, Dy) ions are positioned in the channels formed by the rings. The fundamental building block of α-$(RE)_2B_4O_9$ (RE = Eu, Gd, Tb, Dy) can be specified by the descriptor $20\square{:}[\boxslash\boxbslash] = \langle 4\square\,\boxslash\boxbslash\rangle = \langle 3\square\rangle\square\,| - \langle 5\square\rangle\square\,| = \langle 4\square\,\boxslash\boxbslash\rangle = \langle 3\square\rangle\square\,| - \langle 5\square\rangle\square\,|$. In-situ powder diffraction measurements and DTA investigations showed that the compounds α-$(RE)_2B_4O_9$ (RE = Eu, Gd, Tb, Dy) are stable up to 800 °C. IR and Raman spectroscopy revealed new data for the vibrational behavior of edge-sharing BO_4 tetrahedra. Both α-$Gd_2B_4O_9$ and α-$Tb_2B_4O_9$ exhibit paramagnetism.

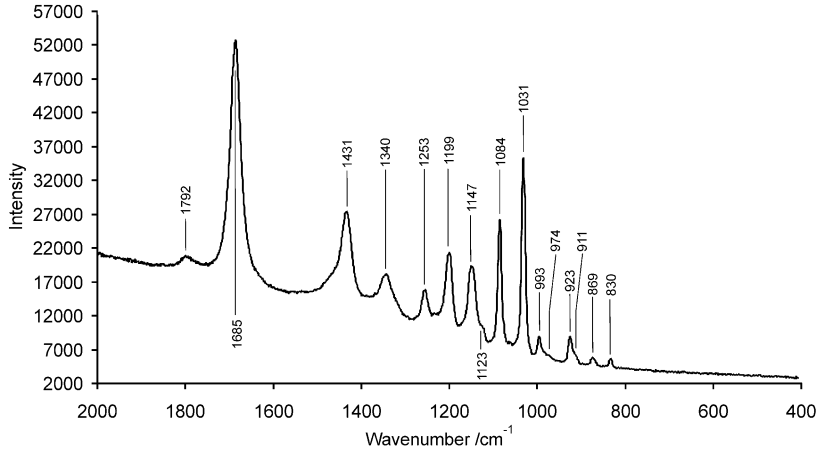

Figure 9. Raman spectrum of α-$Gd_2B_4O_9$.

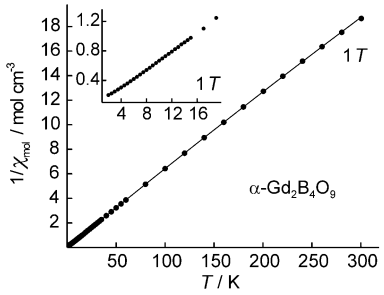

Figure 10. Inverse magnetic susceptibility of α-$Gd_2B_4O_9$.

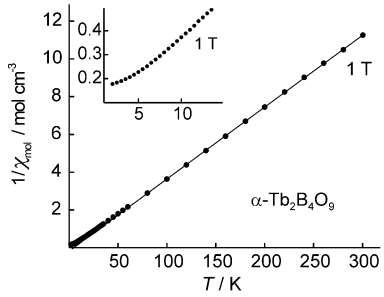

Figure 11. Inverse magnetic susceptibility of α-$Tb_2B_4O_9$.

Table 11. Magnetic parameters of α-$(RE)_2B_4O_9$ (RE = Gd, Tb).

	α-$Gd_2B_4O_9$	α-$Tb_2B_4O_9$
magnetic moment [μ_B per Gd^{3+} or Tb^{3+}]	7.83	10.22
theoretical moment [μ_B per Gd^{3+} or Tb^{3+}]	7.94	9.72
Curie constant	15.342	26.129
paramagnetic Curie temperature [K]	-0.0307	4.7956
χ_0	2.198×10^{-3}	4.406×10^{-4}

Acknowledgement

We gratefully acknowledge the continuous support of these investigations by Prof. Dr. W. Schnick, Department Chemie of the Ludwig-Maximilians-Universität München (Germany). Special thanks go to Prof. Dr. F. Tuczek and U. Cornelissen (Christian-Albrechts-Universität zu Kiel, Germany) for the Raman spectra, to Prof. Dr. R. Pöttgen and M. H. Möller (University of Münster, Germany) for magnetic measurements, to Dr. H. Piotrowski (LMU-München) for collecting the single-crystal data, to Dipl. Min. S. Schmid for DTA, and to Dipl. Chem. S. Correll (LMU-München) for the in-situ powder diffraction measurements. For financial support we thank the Fonds der Chemischen Industrie.

[1] "A Survey of Structural Types of Borates and Polyborates": G. Heller, *Top. Curr. Chem.* **1986**, *131*, 42.
[2] C. L. Christ, J. R. Clark, *Phys. Chem. Minerals* **1977**, *2*, 59.
[3] "The Structural Chemistry of the Borates": V. F. Ross, J. O. Edwards in *The Chemistry Of Boron and its Compounds*, Wiley, New York **1967**.
[4] S. K. Filatov, R. S. Bubnova, *Phys. Chem. Glasses* **2000**, *41*, 216.
[5] H. Huppertz, B. von der Eltz, *J. Am. Chem. Soc.* **2002**, *124*, 9376.
[6] H. Huppertz, *Z. Naturforsch. Teil B* **2003**, *58*, 278.
[7] *Gmelin Handbook of Inorganic and Organometallic Chemistry* C11 b, 8th edition, Springer, Berlin **1991**.
E. M. Levin, R. S. Roth, J. B. Martin, *Am. Mineral.* **1961**, *46*, 1030.
[9] W. F. Bradley, D. L. Graf, R. S. Roth, *Acta Crystallogr.* **1966**, *20*, 283.
[10] J.-Y. Henry, *Mater. Res. Bull.* **1976**, *11*, 577.
[11] R. S. Roth, J. L. Waring, E. M. Levin, *Proc. Conf. Rare Earth Res. 3rd*, **1963**, 153.
[12] G. Chadeyron, M. El-Ghozzi, R. Mahiou, A. Arbus, J. C. Cousseins, *J. Solid State Chem.* **1997**, *128*, 261.
[13] M. Ren, J. H. Lin, Y. Dong, L. Q. Yang, M. Z. Su, L. P. You, *Chem. Mater.* **1999**, *11*, 1576.
[14] K. K. Palkina, V. G. Kuznetsov, L. A. Butman, B. F. Dzhurinskii, *Koord. Khim.* **1976**, *2*, 286.
[15] H. J. Meyer, *Naturwissenschaften* **1969**, *56*, 458.
[16] H. J. Meyer, A. Skokan, *Naturwissenschaften* **1971**, *58*, 566.
[17] H. J. Meyer, *Naturwissenschaften* **1972**, *59*, 215.
[18] M. T. Cohen-Adad, O. Aloui-Lebbou, C. Goutaudier, G. Panczer, C. Dujardin, C. Pedrini, P. Florian, D. Massiot, F. Gerard, C. Kappenstein, *J. Solid State Chem.* **2000**, *154*, 204.
[19] D. A. Keszler, H. Sun, *Acta Crystallogr. Sect. C* **1988**, *44*, 1505.
[20] S. C. Abrahams, J. L. Bernstein, E. T. Keve, *J. Appl. Crystallogr.* **1971**, *4*, 284.
[21] H. Huppertz, *Z. Naturforsch. Teil B* **2001**, *56*, 697.
[22] R. Böhlhoff, H. U. Bambauer, W. Hoffmann, *Z. Kristallogr.* **1971**, *133*, 386.
[23] S. Lemanceau, G. Bertrand-Chadeyron, R. Mahiou, M. El-Ghozzi, J. C. Cousseins, P. Conflant, R. N. Vannier, *J. Solid State Chem.* **1999**, *148*, 229.
[24] J. Weidelt, H. U. Bambauer, *Naturwissenschaften* **1968**, *55*, 342.
[25] G. Canneri, *Gazz. Chim. Ital.* **1926**, *56*, 450.
[26] J. Weidelt, *Z. Anorg. Allg. Chem.* **1970**, *374*, 26.
[27] I. V. Tananaev, B. F. Dzhurinskii, I. M. Belyakov, *Izv. Akad. Nauk SSSR Neorg. Mater.* **1966**, *2*, 1791.
[28] H. U. Bambauer, J. Weidelt, J. St. Ysker, *Z. Kristallogr.* **1969**, *130*, 207.
[29] I. V. Tananaev, B. F. Dzhurinskii, B. F. Chistova, *Izv. Akad. Nauk SSSR Neorg. Mater.* **1975**, *11*, 165.
[30] G. D. Abdullaev, K. S. Mamedov, G. D. Dzhafarov, *Sov. Phys. Crystallogr.* **1975**, *20*, 161.
[31] C. Sieke, T. Nikelski, T. Schleid, *Z. Anorg. Allg. Chem.* **2002**, *628*, 819.
[32] M. Leskelä, L. Niinistö, *Handbook on the Physics and Chemistry of Rare-Earth, Vol. 8* (Eds.: K. A. Gschneider, Jr., L. Eyring), Elsevier Science, Amsterdam, **1986**, p. 203.
[33] J. H. Lin, M. Z. Su, K. Wurst, E. Schweda, *J. Solid State Chem.* **1996**, *126*, 287.
[34] J. H. Lin, S. Zhou, L. Q. Yang, G. Q. Yao, M. Z. Su, *J. Solid State Chem.* **1997**, *134*, 158.
[35] J. H. Lin, L. P. You, G. X. Lu, L. Q. Yang, M. Z. Su, *J. Mater. Chem.* **1998**, *8*, 1051.
[36] H. Huppertz, unpublished results.
[37] P. Becker, *Adv. Mater.* **1998**, *10*, 979.
[38] T. Sasaki, Y. Mori, M. Yoshimura, Y. K. Yap, T. Kamimura, *Mater. Sci. Eng.* **2000**, *30*, 1.
[39] D. A. Keszler, *Curr. Opin. Solid State Mater. Sci.* **1996**, *1*, 204.

[40] H. Huppertz, S. Altmannshofer, G. Heymann, *J. Solid State Chem.* **2003**, *170*, 320.
[41] D. Walker, M. A. Carpenter, C. M. Hitch, *Am. Mineral.* **1990**, *75*, 1020.
[42] D. Walker, *Am. Mineral.* **1991**, *76*, 1092.
[43] D. C. Rubie, *Phase Transform.* **1999**, *68*, 431.
[44] J. W. Visser, *J. Appl. Crystallogr.* **1969**, *2*, 89.
[45] WinX^{POW} Software , STOE & CIE GmbH , Darmstadt **1998**.
[46] W. Herrendorf, H. Bärnighausen, HABITUS, Program for Numerical Absorption Correction, University of Karlsruhe/Giessen (Germany) **1993/1997**.
[47] A. L. Spek, PLATON - A Multipurpose Crystallographic Tool, Utrecht University, Utrecht (The Netherlands), **2002**.
[48] G. M. Sheldrick, SHELXS-97, Program for the Solution of Crystal Structures, University of Göttingen (Germany), **1997**.
[49] G. M. Sheldrick, SHELXL-97, Program for Crystal Structure Refinement, University of Göttingen (Germany), **1997**.
[50] P. C. Burns, J. D. Grice, F. C. Hawthorne, *Can. Mineral.* **1995**, *33*, 1131.
[51] J. D. Grice, P. C. Burns, F. C. Hawthorne, *Can. Mineral.* **1999**, *37*, 731.
[52] W. E. Klee, *Z. Kristallogr.* **1987**, *179*, 67.
[53] A. Beukemann, W. E. Klee, *Z. Kristallogr.* **1994**, *209*, 709.
[54] A. Beukemann, W. E. Klee, *Z. Kristallogr.* **1992**, *201*, 37.
[55] TOPOLAN—Topological Analysis of Crystal Structures, G. Thimm, S. Schumacher, W. Uhr, W. E. Klee, University of Karlsruhe, **1993**.
[56] "Boron: Mineralogy, Petrology, and Geochemistry": F. C. Hawthorne, P. C. Burns, J. D. Grice, *Rev. Mineral.* **1996**, *33*, 42.
[57] I. D. Brown, D. Altermatt, *Acta Crystallogr. Sect. B* **1985**, *41*, 244.
[58] N. E. Brese, M. O'Keeffe, *Acta Crystallogr. Sect. B* **1991**, *47*, 192.
[59] R. Hoppe, *Angew. Chem.* **1966**, *78*, 52; *Angew. Chem. Int. Ed. Engl.* **1966**, *5*, 95.
[60] R. Hoppe, *Angew. Chem.* **1970**, *82*, 7; *Angew. Chem. Int. Ed. Engl.* **1970**, *9*, 25.
[61] R. Hübenthal, MAPLE, Program for the Calculation of MAPLE Values, Vers. 4, University of Giessen (Germany), **1993**.
[62] C. T. Prewitt, R. D. Shannon, *Acta Crystallogr. Sect. B* **1968**, *24*, 869.
[63] J. H. Denning, S. D. Ross, *Spectrochim. Acta* **1972**, *28A*, 1775.
[64] J. P. Laperches, P. Tarte, *Spectrochim. Acta* **1966**, *22*, 1201.
[65] G. Blasse, G. P. M. van den Heuvel, *Phys. Stat. Sol.* **1973**, *19*, 111.
[66] S. D. Ross, *Spectrochim. Acta Part A* **1972**, *28*, 1555.
[67] A. Szytula, J. Leciejewicz, *Handbook of Crystal Structures and Magnetic Properties of Rare Earth Intermetallics*, CRC Press, Boca Raton, FL, **1994**.

Received: December 23, 2002 [F4696]

